

# Adsorption Of Hydrogen Molecules On Carbon Nanotubes Using Quantum Chemistry And Molecular Dynamics

N. Faginas-Lago,<sup>\*,†</sup> D. Oksuz,<sup>†</sup> F. Huarte,<sup>‡</sup> Y. Wang,<sup>¶,§</sup> M. Alcamí,<sup>¶,§</sup> and F.  
Martin<sup>¶,§,||</sup>

<sup>†</sup>*Dipartimento di Chimica, Biologia e Biotecnologie, Università degli Studi di Perugia,  
Via Elce di Sotto 8, 06123 Perugia, Italy*

<sup>‡</sup>*Chemical Physics Department and Institute for Theoretical and Computational Chemistry  
(IQTUB), Universitat de Barcelona, Martí i Franqués 1, 08028 Barcelona, Spain*

<sup>¶</sup>*Departamento de Química, Módulo 13, Universidad Autónoma de Madrid, 28049 Madrid,  
Spain*

<sup>§</sup>*Instituto Madrileño de Estudios Avanzados en Nanociencia (IMDEA-Nanociencia),  
Cantoblanco, 28049 Madrid, Spain*

<sup>||</sup>*Condensed Matter Physics Center (IFIMAC), Universidad Autónoma de Madrid, 28049  
Madrid, Spain*

E-mail: noelia.faginaslago@unipg.it, Tel.: +390755855527

## Abstract

Physisorption and storage of molecular hydrogen on single-walled carbon nanotube (SWCNT) of various diameters and chiralities are studied by means of classical Molecular Dynamics (MD) simulations and a Force Field validated using DFT-D2 and CCSD(T) calculations. A non-rigid carbon nanotube model is implemented with stretching (C-C) and valence angle potentials (C-C-C) formulated as Morse and Harmonic cosine potentials, respectively. Our results evidence that the standard Lennard-Jones potential fails to describe the H<sub>2</sub>-H<sub>2</sub> binding energies. Therefore, our simulations make use of a potential that contains two body term with parameters obtained from fitting CCSD(T)/CBS binding energies. From our MD simulations, we have analyzed the interaction energies, radial distribution functions, gravimetric densities (% wt), and the distances of the adsorbed H<sub>2</sub> layers to the three zigzag type of nanotubes (5,0), (10,0) and (15,0) at 100 and 300 K.

## Introduction

The storage of hydrogen by various new structural forms of carbon which are inherently lightweight materials, has recently gained widespread attention as possible enabling technology of a future hydrogen economy. The continuous increase in the level of hazardous emissions and in the strictness environmental regulations have led to the development of more efficient and safe methods of power generation. Fuel cells, which convert the chemical energy of a fuel into electricity through a chemical reaction with oxygen or another oxidizing agent,<sup>1</sup> emit zero hazardous substances when the fuel is hydrogen, make less noise and have longer life while needing less maintenance. Therefore, they seem to be one of the most promising power generation technologies for the future.<sup>2</sup>

The foremost advantage of hydrogen as an energy source lies in the fact that in addition to being one of the most abundant elements in the universe, it can easily be regenerated. Hydrogen has also other considerable properties. First of all, in fact, hydrogen is the cleanest

fuel and its combustion produces only water vapor and heat reducing so far the emissions of greenhouse gases to a minimum. Second, hydrogen has a chemical energy per mass (141.84 MJ/kg) that is three times larger than that of the most popular chemical fuels, such as liquid hydrocarbons (47.16 MJ/kg).<sup>3</sup> This feature helps meet the global demand for energy as it continues to rise significantly. However, the use of hydrogen as fuel is limited by storage and transportation problems. Hydrogen in fact is the lightest element on earth and is very volatile. Despite its high energy content per mass, it has the disadvantage that the volume of one kg of hydrogen is approximately 10 m<sup>3</sup> under standard conditions. This enormous volume needs to be reduced when looking for practical applications. Due to the fact that hydrogen can only be found in nature mainly as water and hydrocarbons, it has to be produced by purpose when needed from them and this costs three times more than spilling oil.<sup>4</sup>

The currently investigated hydrogen storage technology considered in this paper is the one making use of carbon nanotubes. Carbon nanotubes bear different physical properties depending on their diameter and chirality. The large available volume, particularly in the cavities inside the single walled carbon nanotubes (SWCNTs), can be used for hydrogen storage. It is beneficial to develop storage materials of this type having high capacity, light mass and high stability, which is applicable to movable electronics and moving vehicles. Several recent experiments suggested that SWCNTs are capable of storing hydrogen at ambient temperature and moderate to high hydrogen pressures.<sup>5</sup> Many molecular simulations<sup>6-8</sup> have also been performed to study hydrogen adsorption in SWCNTs. In particular, molecular dynamics (MD) simulations using accurate intermolecular interaction potentials are a powerful tool to describe the highly dynamical adsorption system and to derive useful energetic information at a given temperature.

Many fundamental issues related to the effects of chirality and diameter and how these give rise to the strong H<sub>2</sub> adsorption enthalpy in SWCNT remain to be addressed in detail in order to develop a comprehensive understanding of the overall adsorption phenomenon. Understanding the adsorption mechanism is a key to predict the maximum storage capacity

and to develop a road map for the development of the carbon nanotube (CNT)-based hydrogen storage vehicle. One of these mechanisms is physisorption, mainly dependent on electrostatic and weak van der Waals interactions. Physical adsorption occurs quickly and may be a single-molecule (unimolecular process), a monolayer or several monolayers thick (multi-molecular processes). As physical adsorption takes place, it begins as a monolayer. It can then become multi-layer, and then, if the pores are close to the size of the molecules, more adsorption occurs until the pores are filled with adsorbate. Accordingly, the maximum capacity of a porous adsorbent can be more related to the pore volume than to the surface area. In contrast, chemisorption involves the formation of chemical bonds between the adsorbate and adsorbent is a monolayer, often with a release of heat much larger than the heat of condensation. Desorption of hydrogen chemically bonded to SWCNT requires a temperature higher than 600 K,<sup>9</sup> rendering chemisorption impractical for mobile hydrogen storage.

The goal of this paper is to study the adsorption of molecular hydrogen onto various adsorption sites and orientations on SWCNT in order to estimate the hydrogen storage capacity of carbon nanotubes. The most significant point to be mentioned around these results is that for the SWCNT (15,0) we obtain a gravimetric density (%wt) of 6.70 close to the standard specified by The Department Of Energy (DOE) (i.e 6.5 wt%).<sup>10</sup> The paper is organized as follows. The description of the computational details including the detailed description of the different force fields are given in Section 2, The Molecular Dynamics simulations details and the results obtained are presented and discussed in Section 3. The conclusions are given in the last section.

## Computational Details

The total potential energy used to calculate the total interaction energy for SWCNT and molecular hydrogen,  $V_{total}$ , is obtained as a sum of two intramolecular potentials, one for the

H<sub>2</sub> and the other one for the SWCNT subsystems, and an intermolecular potential,

$$V_{total} = V_{SWCNT} + \sum_{j=1}^n V_{(H_2)_j} + V_{inter} \quad (1)$$

where

$$V_{inter} = \sum_{i=1}^l \sum_{j=1}^n V_{C_i-(H_2)_j} + \sum_{j=1}^{n-1} \sum_{k>j}^n V_{(H_2)_j-(H_2)_k} \quad (2)$$

and  $n$  represents the number of hydrogen molecules and  $l$  the number of C atoms .

## Bonding interactions in SWCNT

During the MD simulations, the nanotubes are no kept rigid and the corresponding intramolecular potential  $V_{SWCNT}$  is computed as a sum of bond length, bond angle, and dihedral potentials:

$$V_{SWCNT} = \sum U(r_{ij}) + \sum U(\theta_{jik}) + \sum U(\phi) \quad (3)$$

The stretching of C–C bond in SWCNT is formulated as a Morse potential:

$$U(r_{ij}) = E_0[\{1 - \exp(-k(r_{ij} - r_0))\}^2 - 1] \quad (4)$$

where  $r_{ij}$  is the distance between C atoms  $i$  and  $j$ , the parameters are as follows:  $E_0 = 114.4569 \text{ kcal mol}^{-1} \text{ \AA}^{-2}$ ,  $r_0 = 1.418 \text{ \AA}$  and  $k = 2.1867 \text{ \AA}^{-1}$ . Valence angle potentials for the bond bending between C–C–C atoms of SWCNT are described by a harmonic cosine function:

$$U(\theta_{jik}) = \frac{k}{2}(\cos(\theta_{jik}) - \cos(\theta_0))^2 \quad (5)$$

where  $\theta_{jik}$  is the angle between atoms  $C_j$ - $C_i$ - $C_k$ , and the parameters<sup>11</sup> are  $\theta_0=120^\circ$  and  $k = 134.5 \text{ kcal mol}^{-1}$ . The dihedral potential energy term describing the torsional interactions in the carbon nanotube is computed by taking the general triple cosine function<sup>11</sup>

$$U(\phi) = \frac{1}{2}A_1(1 + \cos(\phi)) + \frac{1}{2}A_2(1 - \cos(2\phi)) + \frac{1}{2}A_3(1 + \cos(3\phi)) \quad (6)$$

where  $\phi$  is the dihedral angle among the four C atoms, and reducing it to a simpler functions using parameters  $A_1= 0$ ,  $A_2= 6.009569 \text{ kcal mol}^{-1}$  and  $A_3= 0$ .

## H<sub>2</sub>-SWCNT interaction

For the SWCNT-H<sub>2</sub> interaction, we have carried out systematic DFT-D2<sup>12</sup> calculations for the binding energy of the H<sub>2</sub>-(5,0)-SWCNT complex, with different molecular orientations, distances and adsorption sites. The nanotube used is made of 20 carbon atoms per unit cell. The calculations were performed using the Vienna Ab initio Simulation Package (VASP) employing the generalized gradient corrections (GGA) of Perdew-Burke-Ernzerhof (PBE) functional.<sup>13</sup> The Grimme's DFT-D2 method was employed to describe the long-range vdW interactions, which are described using the following formula:

$$E_{disp} = -s_6 \sum_{i=1}^{N_{at}} \sum_{j=i+1}^{N_{at}} \left( \frac{C_{ij}^6}{R_{ij}^6} f_{dmp}(R_{ij}) \right). \quad (7)$$

where  $N_{at}$  is the number of atoms in the system,  $C_{ij}^6$  the dispersion coefficient for atom pairs  $i$  and  $j$ ,  $s_6$  a global scaling factor,  $R_{ij}$  the interatomic distance between atoms  $i$  and  $j$ , and  $f_{dmp}$  a damping function. In Eq. 7, the scaling parameter  $s_6$  in the DFT-D2 scheme was set to be 0.6 (in stead of the default value 0.75), which has been calibrated based on our CCSD(T)/CBS binding energy calculations for the H<sub>2</sub>-benzene system.

The binding energies from CCSD(T) computations at the CBS limit have been extrapolated using the binding energies from CCSD(T) and MP2 computations with two basis sets, aug-cc-pVDZ and aug-cc-pVTZ,<sup>14</sup> and by assuming that the difference between CCSD(T) and MP2 binding energies remains constant at such large basis sets.<sup>15</sup>

The binding energy between the hydrogen molecule and the SWCNT has been calculated for different molecular orientations and adsorption sites of H<sub>2</sub> and distances (R) between the H<sub>2</sub> and the SWCNT (see Fig. 1), with R being the distance of the center of mass of the hydrogen molecule from the nanotube center. For each geometry and adsorption site, we calculated the energy value by varying the intermolecular distance R, from 4 to 8 Å in steps of 0.2 Å. Our calculations have been carried out using the periodic boundary conditions, so the carbon nanotube is infinitely long.

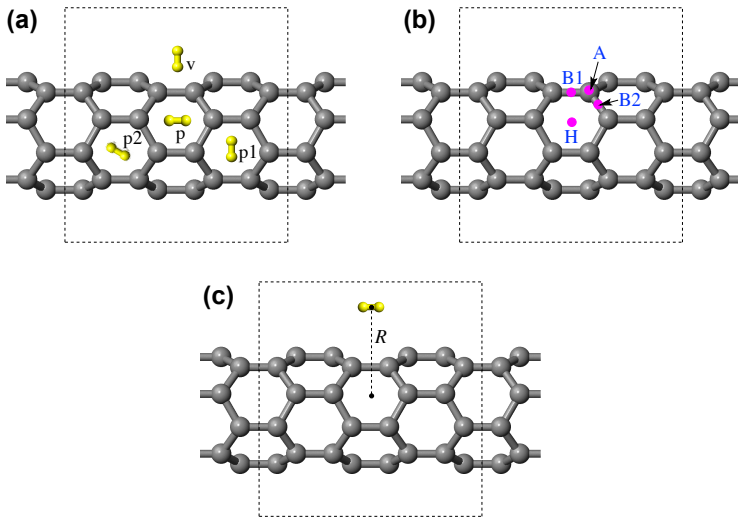


Figure 1: (a) Typical orientations of H<sub>2</sub> around SWCNT. Adsorption sites of H<sub>2</sub> on SWCNT. (c) Distance R between centers of mass of H<sub>2</sub> molecule and SWCNT. All calculations have been carried out using periodic boundary conditions. Dashed boxes indicate the unit cell of the periodic models.

Hydrogen is placed above a carbon atom (site A), above the center of a hexagon of carbon atoms (site H), and above the midpoint of a C-C bond site B1 and B2, respectively and four different orientations (p, p1, p2 and v), given a total of sixteen geometries considered. In this case, a total of sixteen geometries were considered. Among these geometries, it is observed

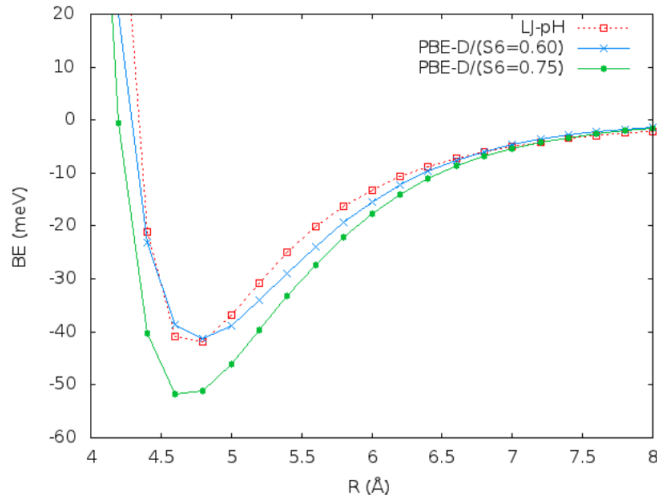


Figure 2: Binding energies of hydrogen with SWCNT for the pH configuration

that the most stable arrangement is the one with the  $\text{H}_2$ -axis parallel to the nanotube axis and sitting on the hollow site of nanotube (pH-configuration).

A Lennard-Jones (LJ) potential has been used to describe intermolecular interaction between  $\text{H}_2$  and the carbon atoms in the SWCNT in the MD calculations, as follows:

$$U(r_{ij}) = 4\epsilon \left[ \left( \frac{\sigma}{r_{ij}} \right)^{12} - \left( \frac{\sigma}{r_{ij}} \right)^6 \right] \quad (8)$$

where  $r_{ij}$  represents the distance between atoms  $i(\text{H})$  and  $j(\text{C})$ , and the parameters  $\epsilon$  and  $\sigma$  were fitted from density functional theory (DFT) calculations. Accordingly, we performed, first, CCSD(T) calculations at complete basis set (CBS)<sup>16</sup> limit for the  $\text{H}_2$ -benzene systems. Then DFT calculations were extended to the  $\text{H}_2$ -SWCNT systems with BSSE correction included. The fitted LJ parameters from the DFT-D2 calculations are:  $\epsilon = 0.0360 \text{ kcal mol}^{-1}$  and  $\sigma = 3.02 \text{ \AA}$ . Fig. 2 shows the binding energies of hydrogen with SWCNT for the pH configuration, and we can see that the LJ potential nicely reproduces of the overall DFT-D2 results.

## H<sub>2</sub>-H<sub>2</sub> interaction

The covalent H-H bond was modeled by the Morse potential given by Eq. 3. The values of the parameters used in our calculation are as follow:<sup>11</sup>  $E_0 = 109.20 \text{ kcal mol}^{-1} \text{ \AA}^{-2}$ ,  $r_0 = 0.746 \text{ \AA}$  and  $k = 3.52 \text{ \AA}^{-1}$ . For the H<sub>2</sub>-H<sub>2</sub> interaction, CCSD(T)/CBS calculations<sup>16</sup> have been performed for the H<sub>2</sub> dimer. The H<sub>2</sub>-H<sub>2</sub> binding energies were calculated for different configurations of the hydrogen molecules (see Fig. 3). For each configuration, we calculated binding energies by varying the intermolecular distance R, from 2 to 4 \AA in step of 0.1 \AA. The most stable configuration corresponds to the v-shaped configuration in which an H<sub>2</sub>-axis points perpendicularly to the other H<sub>2</sub> axis. The LJ potential results show that p1-shaped geometry is the most stable configuration with the two H<sub>2</sub> molecules parallel (see Fig. 4). The parameters employed for the H<sub>2</sub>-H<sub>2</sub> interaction using a Lennard-Jones potential (represented in Fig. 4) are  $\sigma = 2.81 \text{ \AA}$  and  $\epsilon = 0.01707 \text{ kcal mol}^{-1}$ .

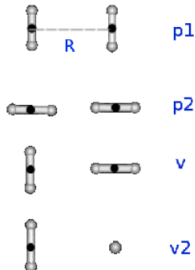


Figure 3: Different configurations of H<sub>2</sub> dimer.

In Fig. 4, the binding energy curves are plotted for the most stable configurations according to CCSD(T)/CBS and LJ potential results (p1 and v-shaped). As shown by Fig. 4, the LJ empirical values are not consistent with CCSD(T)/CBS binding energies. We have found that the LJ potential fails to describe the obtained H<sub>2</sub>-H<sub>2</sub> binding energies. Therefore, in order to apply an analytic potential for the H<sub>2</sub>-H<sub>2</sub> interactions, we have employed a more sophisticated potential containing two-body term with parameters obtained by fitting to the CCSD(T)/CBS binding energies. This potential is a combination of a Morse potential and

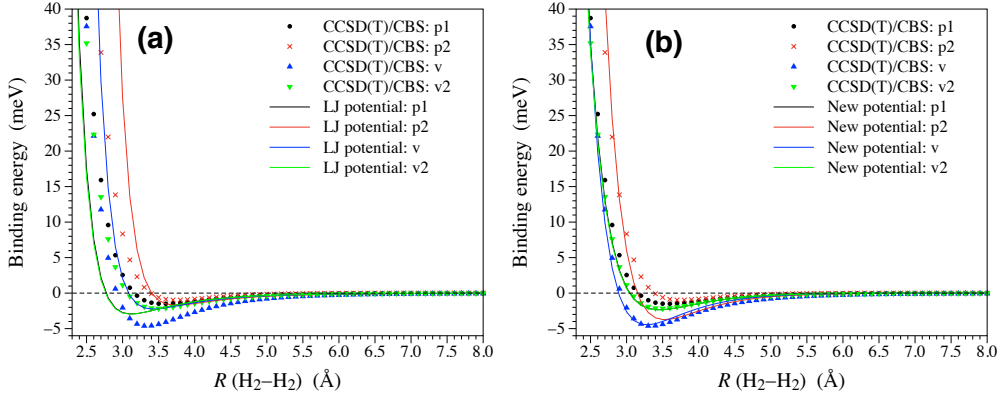


Figure 4: (a) Comparison of binding energies of H<sub>2</sub> dimer with different configurations, between results obtained from the LJ potential and from the CCSD(T)/CBS computations. (b) Comparison of binding energies of H<sub>2</sub> dimer with different configurations, between results obtained from our new potential (Eq. 8) and from the CCSD(T)/CBS computations.

a screened harmonic potential, as written in the following:

$$U(r_{ij}, r_{i\mu}, r_{i\nu}, \theta_{\mu i\nu}) = E_0 \{ [1 - \exp(-k_1(r_{ij} - r_0))]^2 - 1 \} + \frac{k_2}{2} (\theta_{\mu i\nu} - \theta_0) \exp(r_{i\mu}/\rho_1 - r_{i\nu}/\rho_2) \quad (9)$$

where  $r_{ij}$  is the distance between hydrogen atom  $i$  and  $j$ ,  $r_{i\mu}$  the distance between hydrogen  $i$  and the center of the first H<sub>2</sub> molecule (represented by X)  $\mu$ ,  $r_{i\nu}$  the distance between hydrogen  $i$  and the center of the second H<sub>2</sub> molecule  $\nu$ ,  $\theta_{\mu i\nu}$  the angle defined by  $\mu$ - $i$ - $\nu$ . The parameters obtained by fitting to the CCSD(T)/CBS binding energies are listed in Table 1.

**Table 1: Fitted parameters for the H<sub>2</sub>-H<sub>2</sub> potential.**

$E_0$ (kcal mol <sup>-1</sup> Å <sup>-2</sup> )	$r_0$ (Å)	$k_1$ (Å <sup>-1</sup> )	$k_2$ (Å <sup>-1</sup> )	$\theta_0$ (rad.)	$\rho_1$ (Å)	$\rho_2$ (Å)
0.0135	3.489	1.713	-1800.0	1.5708	0.33	0.33

Our CCSD(T) binding energies of H<sub>2</sub> dimer are consistent with the ab initio data in the literature.<sup>17,18</sup> The binding energy order between different configurations of H<sub>2</sub> dimer, the equilibrium intermolecular distances and the corresponding minimum binding energies are all in good agreement with previous work (see the above-mentioned references).

# Molecular Dynamics simulations

Our MD simulations were performed considering a microcanonical ensemble of particles (NVE) enforcing parallelepiped periodic boundary conditions using the DL\_POLY<sup>19</sup> classical dynamics program, at two different temperatures 100 and 300 K. Each MD trajectory is equilibrated for 0.3 ns and then propagated for another 1 ns, with a time step of  $2.5 \times 10^{-4}$  ps. A cutoff radius of 10.0 Å is applied to the non-bonding interactions in order to speed up the computation. The data collected along the 1 ns of equilibration is excluded from the statistical analysis performed at the end of the MD trajectory. Energy contributions, radial distribution functions (RDFs) and gravimetric densities (% wt), as a function of the temperature and of the H<sub>2</sub> concentration, have been analyzed.

In the present investigation, we have used the Tubebash script<sup>20</sup> to construct the SWCNT structure. To examine the maximum capacity for hydrogen storage inside SWCNT's in this work we report detailed molecular dynamics simulation results for hydrogen molecules into a (5,0), (10,0) and (15,0). To investigate the effect of the H<sub>2</sub> loading, we considered a zigzag nanotubes made of five unit cells and 100, 200 and 300 carbon atoms for (5,0), (10,0) and (15,0) SWCNTs, respectively. The simulation are performed at 100 K and 300 K with parallelepiped periodic boundary conditions. The diameter (d) of the SWCNT is calculated using the following expression

$$d = \frac{a}{\pi} \sqrt{(n^2 + nm + m^2)} \quad (10)$$

where  $a = 0.246$  nm and (n,m) are the chiral vector of SWCNT. After the SWCNT structure was obtained, H<sub>2</sub> molecules were added randomly around the SWCNT at a distance varying from 4 and 8 Å. The criterium used to decide of the H<sub>2</sub> molecules were physisorbed if the distance of the H<sub>2</sub> molecule of mass (c.o.m) is smaller than 3 Å and any SWCNT carbon atom.

In order to analyze the effect of the various parameters of the MD simulation on the distri-

bution of adsorbed hydrogen molecules, we first determined the amount of adsorbed  $H_2$  at the endohedral and exohedral sites of the SWCNT. To understand the dependence of the  $H_2$  distribution on the diameter of the nanotube, SWCNTs of different diameters were selected. Then, the dependence of the radial distribution function was analyzed in order to figure out the composition of attractive and repulsive interaction between  $H_2$  molecules and SWCNT. The effect of temperature on  $H_2$  distribution was also investigated.

The simulation results for each nanotube are showed in Table 2, where  $N_c$  is the number of carbon atoms. Table 2 lists the number of hydrogen molecule adsorbed in exohedral ( $N_{H_2,out}$ ) and endohedral ( $N_{H_2,in}$ ) sites for the three types of SWCNT. In all runs the same number of initial  $H_2$  molecules has been employed, all distributed randomly around the nanotube. It is important to notice that not all the  $H_2$  molecules are adsorbed.

**Table 2: Results of the  $H_2$  molecular adsorbed as a function of the temperature and the chirality.**

SWCNT	d(Å)	$N_c$	T(K)	$N_{H_2,in}$	$N_{H_2,out}$
(5,0)	3.914	100	96.51	0	7
(5,0)			251.01	0	1
(10,0)	7.828	200	92.20	7	22
(10,0)			274.01	5	16
(15,0)	11.743	300	100.93	33	45
(15,0)			287.02	21	9

As an illustrative example of the equilibrium, Fig. 5 shows the system configuration after 1 ns of simulation in the (15,0) case.

We have observed that the  $H_2$  population distribution at the endohedral(in) and exohedral(out) sites increases with the diameter of nanotube due to fact that the volume of both exohedral and endohedral sites increases as the nanotube diameter becomes larger.

The distribution of hydrogen molecules around the SWCNT could be extracted from the radial distribution function (RDF),  $g(r)$ . This function is defined as the probability of finding molecular hydrogens at distance  $r$  from the nanotube surface, relative to the probability expected for a completely random distribution at the same density of  $H_2$ . The RDF is of

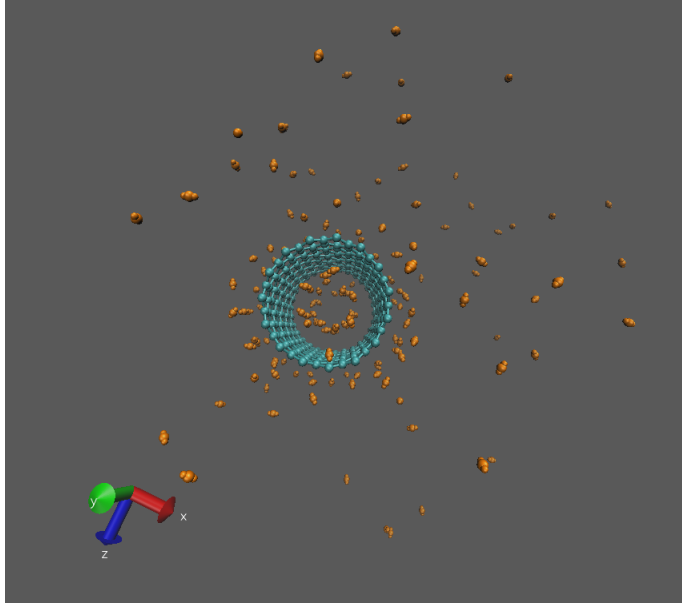


Figure 5: Snapshot of final configuration with 100 H<sub>2</sub> molecules for the (15,0).

particular importance since it can be extracted from neutron scattering measurements and compared with the values obtained is plotted for both C-X and X-X pairs for the already mentioned three types of SWCNT. Figures 6 and 7 show the C-X RDF for the three types of SWCNT considered at T=100 K and 300 K, respectively. One can see sharp rise of  $g(r)$  at  $r \approx 3 \text{ \AA}$ , which is the distance of closest approach of H<sub>2</sub> molecules to the surface of SWCNTs, thus suggesting a pure physisorption mechanism. The rise is followed by a strong (for (10,0) and (15,0)) or a slight (for (5,0)) plateau. The position of the peaks reflects the average relative position between SWCNT and hydrogen. The first peak is located at around  $3 \text{ \AA}$  while the second peak is around  $8 \text{ \AA}$ . From these plots we deduce that the higher the temperature, the less H<sub>2</sub> adsorbed. Fig. 8 shows the RDF of the H<sub>2</sub> molecules for the two different temperatures (100 and 300 K). The first peak occurs at X-X distances between  $3.2$  and  $3.6 \text{ \AA}$  for different SWCNT, and mainly reflects the attractive interaction between H<sub>2</sub> molecules. However, when the temperature increase (dashed lines) the RDF of the SWCNT (10,0) and (15,0) show a bimodal structure.

Using the data in Table 2 we have also been able to analyze the effect of the temperature in the hydrogen distribution. Table 2 shows that, for the same nanotube diameter, the

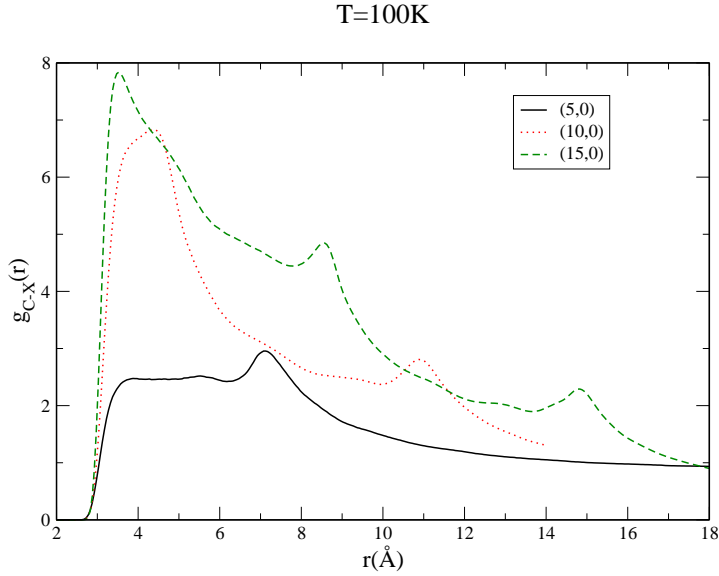


Figure 6: Radial distribution function between C atoms and c.o.m of hydrogen molecular, represented by X at T=100 K for the three SWCNT considered. Full line (5,0), dotted line (10,0) and dashed line (15,0).

number of  $\text{H}_2$  molecules adsorbed both inside and outside the nanotube decreases with the temperature. As the temperature increases, the interaction energy decreases, reducing the strength of C and H atom interaction.

In order to provide the graphical evidence with a more qualitative ground we calculated also the storage capacity for three types of zigzag ((5,0), (10,0) and (15,0)) open-ended SWCNTs at the two different temperatures of 100 K and 300 K. To this end the nanotubes were progressively loaded with hydrogen by carrying out consecutive molecular dynamics simulations till saturation of the nanotube. In all cases, for the three types of SWCNT analyzed, 100  $\text{H}_2$  molecules were distributed randomly around it as an initial run. Then, the simulation was run and adsorption of the  $\text{H}_2$  on the SWCNT was analyzed. If the nanotube was not saturated, the adsorbed hydrogen molecules were conserved and a new group of 100  $\text{H}_2$  molecules was added under the same initial conditions. Gravimetric density is calculated at every step of the trajectory using

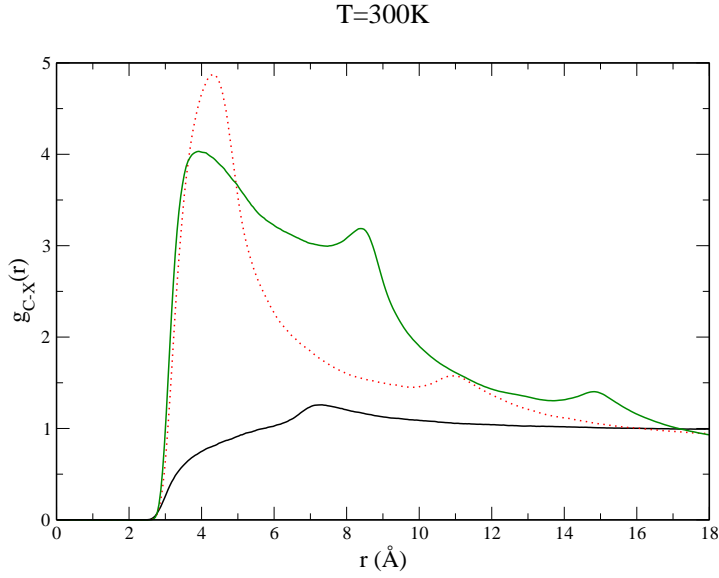


Figure 7: Radial distribution function between C atoms and c.o.m of hydrogen molecular, represented by X at T=300 K for the three SWCNT considered. Full line (5,0), dotted line (10,0) and dashed line (15,0).

$$wt(\%) = \frac{N_a M_{H_2}}{N_a M_{H_2} + M_{adsorbent}} \times 100 \quad (11)$$

where  $N_a$  is the number of adsorbed molecules for a given number of molecules in the gas phase  $N$ . The molecules adsorbed are estimated by counting those that are located at a distances of 3 Å from the surface of the SWCNT.  $M_{adsorbent}$  is the mass of the adsorbent. Hydrogen storage capacity (HSC) indicates the amount of gas that can occupy a given volume as a result of any additional hydrogen storage effect with respect to the amount of gas occupying the same volume at constant temperature.<sup>21</sup> In other words, HSC is the capacity of storing hydrogen shown by a material, in a addition to that of a compression of the gas at the same pressure and temperature. HSC is most commonly expressed as weight percent (wt%) of the stored gas over the sum of the weight of the adsorbed gas and the adsorbent.

Fig. 9 shows the wt% for the consecutive simulations of the progressive loading procedure

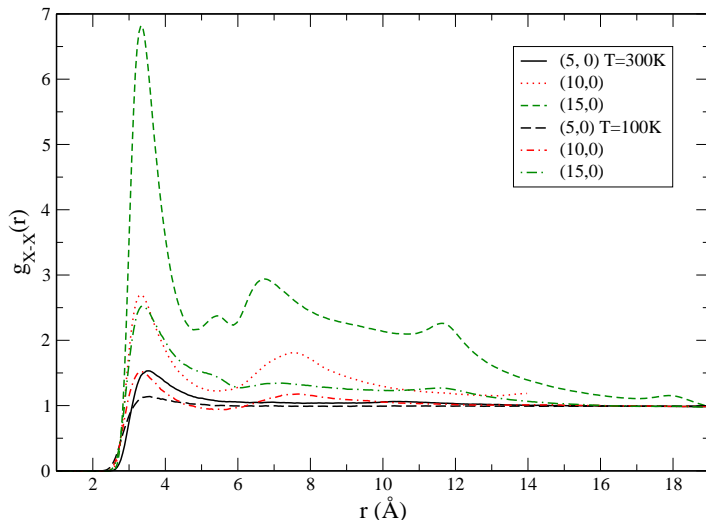


Figure 8: Radial distribution function for H-H separation at intermolecular distance.

for the (10,0) nanotube at 100 K. In this figure, each panel corresponds to one simulation of the related type of nanotube. For the medium diameter nanotube (10,0) the progressive loading was repeated up to six times, getting saturation of the nanotube. The results of the six simulations are shown in Fig. 9. The calculated storage capacity is 2.40 wt%. For the nanotube with the largest diameter (15,0), the simulations were repeated up to four times till saturation of the nanotube. In this case, the calculated a storage capacity is 6.7 wt%. The same procedure was followed for the three types of SWCNT by raising the temperature to 300 K.

After saturating the SWCNTs, we analyzed the distribution of the  $H_2$  molecules around the nanotube. To simplify the analysis we set the Z coordinate constant and plotted the probability density map. The map shows therefore the probability of finding the  $H_2$  molecules placed around the nanotube, on the XY-plane (see Fig. 10 for this xy-plane projected distribution of the  $H_2$  for the three types of SWCNTs at 100 K). In the case of the nanotube with the smallest nanotube (top-left), the density map shows that the highest probability of finding the  $H_2$  molecules corresponds to a crown around the SWCNT (yellow region). In

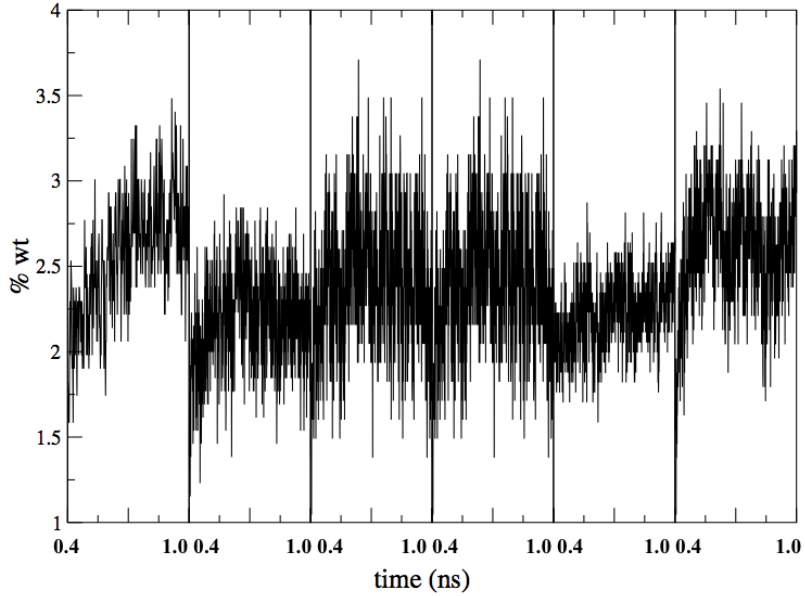


Figure 9: The hydrogen gravimetric density (wt%) plotted as a function of time for (10,0) SWCNT at 100 K. Each rectangle represents a simulation during the data collect time of 1 ns.

the case of (10,0) and (15,0) nanotubes (top-right and bottom), it is observed that as the nanotube diameter increases, the maximum of the probability shifts inside the nanotube.

The final  $H_2$  storage capacities of the three types of SWCNT are listed in Table 3 in terms of gravimetric densities (wt%), for the temperatures of 100 and 300 K. As expected, the maximum storage of  $H_2$  is obtained for the nanotube (15,0) since it has the largest diameter (and, therefore, the largest volume). We note also that as the temperature increases, the  $H_2$  storage capacity decreases due to fact that hydrogen molecules are increasingly desorbed. We can explain this effect of the temperature in terms of a decrease of the van der Waals (intermolecular) energy (see Table 3) that leads to the weakening of the interaction between C and H atoms.

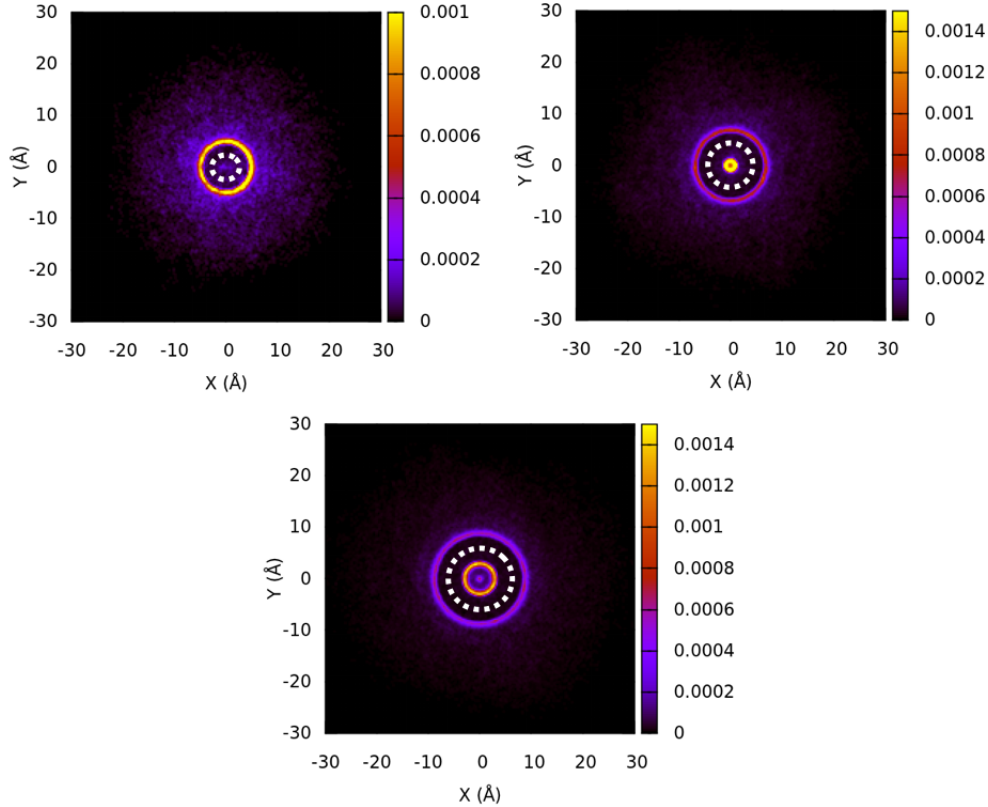


Figure 10: Density map for (5,0) at left upward, (10,0) at right-upward and (15,0) at bottom panel at 100K. The SWCNT walls are indicated in the figure by dotted white lines.

## Conclusions

In this paper we have systematically investigated the  $H_2$  storage capacity of SWCNTs using a classical MD technique. As demonstrated by our MD calculations, the highest hydrogen storage capacity is obtained for the nanotube with the largest diameter, owing to the fact that high surface area favors adsorption of  $H_2$  molecules. The other crucial observation is that as the temperature increases, the  $H_2$  storage capacity decreases since the interaction between SWCNT and  $H_2$  weakens, thus favoring desorption of  $H_2$  molecules. For low  $H_2$  densities,  $H_2$  tends to adsorb in the exohedral sites. As the  $H_2$  loading increases, the endohedral sites become more populated. The larger nanotube diameter (15,0) provides the the highest relative population in the endohedral sites but never exceeds the population adsorbed in the exohedral sites. In contrast to many reported classical MD simulations,<sup>5,22,23</sup>

**Table 3: The VdW Energies (kcal/mol) for the three different SWCNTs at T=100K and 300 K. Also listed the gravimetric density (wt%) results.**

SWCNT	d (Å)	$E_{vdW}$ 100 K	$E_{vdW}$ 300 K	wt% 100 K	wt% 300 K
(5,0)	3.914	-6.9979	-2.0395	0.61	0.086
(10,0)	7.828	-36.064	-15.745	2.40	1.37
(15,0)	11.743	-77.317	-30.544	6.70	2.58

the LJ parameter,  $\epsilon$  (the depth of the potential well), corresponding to the C-H<sub>2</sub> interaction is defined as independent of the nanotube curvature. DFT-D2 calculations show that, in the case of SWCNT-H<sub>2</sub>, parallel adsorption sites are more stable than perpendicular configurations, and for external adsorption, the hollow site is preferable over the other sites. These results are also consistent with the studies of W. J. Fan et al.<sup>22,23</sup> This justifies the use of the LJ potential to describing the H<sub>2</sub>-SWCNT interaction using MD simulations. However, the LJ empirical potential is not accurate enough to describe H<sub>2</sub>-H<sub>2</sub> interaction.

## Acknowledgement

Noelia Faginas Lago acknowledges financial support from Phys4entry FP72007-2013 (contract 242311). The computing for this project (MD calculations) was performed at the OU Supercomputing Center for Education & Research (OSCER) at the University of Oklahoma (OU). Work also supported by the MINECO projects FIS2013-42002-R and CTQ2013-43698-P, the CAM project NANOFRONTMAG-CM (ref. S2013/MIT-2850), the MINECO project FUNCGRAPHENE (ref. FIS2013-40667-P) and the European COST Action CM1204 XLIC.

## References

- (1) Khurmi, R. S.; Sedha, R. S. *Materials Science*; S. Chand & Company Ltd: New Delhi, 2012.

- (2) Atay, G. An Investigation of Hydrogen Storage in Carbon Nanotubes via Computational MM Methods. 2005; Bogazici University.
- (3) Züttel, A. Hydrogen storage methods. *Naturwissenschaften* **2004**, *91*, 157–172.
- (4) Zhou, L. Progress and problems in hydrogen storage methods. *Renewable and Sustainable Energy Reviews* **2005**, *9*, 395 – 408.
- (5) Cheng, H.; Cooper, A. C.; Pez, G. P.; Kostov, M. K.; Piotrowski, P.; ; Stuart, S. J. Molecular Dynamics Simulations on the Effects of Diameter and Chirality on Hydrogen Adsorption in Single Walled Carbon Nanotubes. *The Journal of Physical Chemistry B* **2005**, *109*, 3780–3786, PMID: 16851425.
- (6) Wang, Q.; Johnson, K. Molecular Simulation of Hydrogen Adsorption in Single-Walled Carbon Nanotubes and Idealized Carbon Slit Pores. *J. Chem. Phys.* **1999**, *110*, 577–586.
- (7) Darkrim, F.; Levesque, D. Monte Carlo simulations of hydrogen adsorption in single-walled carbon nanotubes. *The Journal of Chemical Physics* **1998**, *109*, 4981–4984.
- (8) Wang, Q.; ; Johnson\*, J. K. Optimization of Carbon Nanotube Arrays for Hydrogen Adsorption. *The Journal of Physical Chemistry B* **1999**, *103*, 4809–4813.
- (9) Liu, C. F.; Y.Y. Liu, M.; Cong, H.; Cheng, H.; Dresselhans, M. Hydrogen Storage in Single-Walled Carbon Nanotubes at Room Temperature. *Science* **1999**, *286*, 1127–1129.
- (10) Hirscher, M.; Becher, M.; Haluska, M.; von Zeppelin, F.; Chen, X.; Dettlaff-Weglikowska, U.; Roth, S. Are carbon nanostructures an efficient hydrogen storage medium? *Journal of Alloys and Compounds* **2003**, *356*–*357*, 433 – 437, Proceedings of the Eighth International Symposium on Metal-Hydrogen Systems, Fundamentals and Applications (MH2002).

- (11) Huarte-Larrañaga, F.; Albertí, M. A molecular dynamics study of the distribution of molecular hydrogen physisorbed on single walled carbon nanotubes. *Chemical Physics Letters* **2007**, *445*, 227–232.
- (12) Grimme, S. Semiempirical GGA-type density functional constructed with a long-range dispersion correction. *Journal of Computational Chemistry* **2006**, *27*, 1787–1799.
- (13) Perdew, J. P.; Burke, K.; Ernzerhof, M. Generalized Gradient Approximation Made Simple. *Phys. Rev. Lett.* **1996**, *77*, 3865–3868.
- (14) Grabowski, S. J.; Sokalski, W. A.; Leszczynski, J. How Short Can the H<sub>2</sub>-H<sub>2</sub> Intermolecular Contact Be? New Findings that Reveal the Covalent Nature of Extremely Strong Interactions. *The Journal of Physical Chemistry A* **2005**, *109*, 4331–4341, PMID: 16833763.
- (15) Hobza, P. Theoretical studies of hydrogen bonding. *Annu. Rep. Prog. Chem., Sect. C: Phys. Chem.* **2004**, *100*, 3–27.
- (16) Truhlar, D. G. Basis-set extrapolation. *Chemical Physics Letters* **1998**, *294*, 45–48.
- (17) Wind, P.; Røeggen, I. A theoretical study of the (H<sub>2</sub>)<sub>2</sub> dimer. II. The potential energy surface. *Chemical Physics* **1992**, *167*, 263 – 275.
- (18) Diep, P.; Johnson, J. K. Erratum: An accurate H<sub>2</sub>-H<sub>2</sub> interaction potential from first principles. *The Journal of Chemical Physics* **2000**, *113*, 3480–3481.
- (19) Smith, W.; Yong, C.; Rodger, P. DL\_POLY: Application to molecular simulation. *Molecular Simulation* **2002**, *28*, 385–471.
- (20) White, C. T.; Robertson, D. H.; Mintmire, J. W. Helical and rotational symmetries of nanoscale graphitic tubules. *Phys. Rev. B* **1993**, *47*, 5485–5488.

- (21) Chen, P.; Zhang, H.-B.; Lin, G.-D.; Hong, Q.; Tsai, K. Growth of carbon nanotubes by catalytic decomposition of {CH<sub>4</sub>} or {CO} on a NiMgO catalyst. *Carbon* **1997**, *35*, 1495–1501.
- (22) Knippenberg, M. T.; Stuart, S. J.; Cheng, H. Molecular dynamics simulations on hydrogen adsorption in finite single walled carbon nanotube bundles. *Journal of Molecular Modeling* **2008**, *14*, 343–351.
- (23) Fan, W. J.; Zhang, R. Q.; Teo, B. K.; Aradi, B.; Frauenheim, T. Prediction of energetically optimal single-walled carbon nanotubes for hydrogen physisorption. *Applied Physics Letters* **2009**, *95*.

# Graphical abstract

